



Efficient photocatalytic activity of Au@Mg nanospheres on mineralization of polystyrene: A sustainable remediation strategy on sunlight-induced photodegradation, environmental toxicity, and sensing of cefixime

S. Balasurya^a, Abdullah A. AL-ghamdi^a, Mohammad K. Okla^{a,*}, Saud A. Al-amri^a, Mostafa A. Abdel-Maksoud^a, Mohammed Aufy^b, S. Sudheer Khan^{c,*}

^a Botany and Microbiology Department, College of Science, King Saud University, P.O. Box 2455, Riyadh 11451, Saudi Arabia

^b Department of Pharmaceutical Sciences, Division of pharmacology and Toxicology, University of Vienna, Austria

^c Centre for Energy, Materials and Telecommunications, Institut National de la Recherche Scientifique, Varennes, QC, Canada.

ARTICLE INFO

Keywords:

Au@Mg nanospheres
Photocatalytic degradation
Polystyrene
Detection of cefixime

ABSTRACT

The overexploitation of synthetic plastic materials has led to their accumulation in various ecosystems. This causes serious ailments and existential threat to biological entities of numerous hierarchical categories. The Au@Mg nanospheres were fabricated by ascorbic acid chemical reduction method and this material serves as a potential tool to mineralise plastic materials. TEM imaging of Au@Mg implies the Mg at core and Au at shell. The photocatalytic degradation of Au@Mg on polystyrene was studied and the effective degradation was found to be 97.1 %. The reusability of Au@Mg nanosphere was studied and the reusability efficiency was found to be 99.5 %. The OCl[•] and •OH radical plays a major role in the photocatalytic degradation of polystyrene. In addition, the good sensing assay on the detection of cefixime (CEF) was studied and it shows selective and sensitive detection towards CEF. The limit of detection of CEF by Au@Mg nanospheres was calculated to be 450 pM. The selectivity of the probe was further studied by interference and it has been observed that the detection was effective only in presence of CEF with metal drug mixture. In addition, the good sensing of Au@Mg nanospheres towards cefixime was studied by spiking it with blood serum and the recovery percentage was calculated to be 99.7 %. Genotoxicity of the polystyrene on *Allium cepa* was performed before and after degradation and the results didn't show any toxicity by the degraded product. Thus, the prepared bimetallic Au@Mg nanosphere serves as an effective sensor for the monitoring and optimization of CEF drug for the treatment of various microbial infections in human and as an effective photocatalytic material for the degradation of polystyrene.

1. Introduction

Antibiotics had been widely used in the treatment of various bacterial infections [1]. However, its wide application and long-term consumption of drug leads to health implications [1,2]. Among the wide spectrum of antibiotics, cefixime (CEF) had its application on the treatment of microbial infection in tonsillitis, urinary tract infections, throat infections, bronchitis and middle ear infections [3]. In addition, the cephalosporin antibiotics (cefixime) show admirable effect against vulnerable gram-positive and gram-negative bacteria [3,11].

It is essential to optimize the drug concentration against microbial infection. Several analytical methods were used for the qualitative and quantitative analysis of CEF such as, capillary electrophoresis, chro-

matography, spectrophotometry, electrochemical methods and spectrophotometric method [4–8]. According to the previous literature, the method employed for the effective quantification of CEF was found to be complicated instrumentation, expensive, application of toxic organic solvents and low sensitivity [9–12]. Hence, there is an urgent need to develop a stable, reproducible and good sensing tool for the effective quantification of CEF [13–16].

Plastic contamination has been a major threat over decades and processing them into non-toxic pollutants is an essential need [17]. According to the previous literature, semiconductor nanomaterial was widely used in the photocatalytic application on the removal of toxic pollutant from environmental water bodies [18–21]. Spectrophotometric tool had been widely used in the sensing of various analyte including, an-

* Corresponding authors.

* Corresponding authors.

E-mail addresses: malokla@ksu.edu.sa (M.K. Okla), sudheer.k-sulfath@inrs.ca

<https://doi.org/10.1016/j.jwpe.2022.103350>
Received 26 July 2022; Received in revised form 27 October 2022; Accepted 13 November 2022
2214-7144/© 20XX

tibiotics, heavy metals, biological fluids and also for the photocatalytic degradation of various pollutants [22–24]. Here, Ag and Au based nano sensors have been widely used in the sensing application owing to its surface plasmon resonance (SPR) property [24–26]. Au and Ag based nanomaterial has its wide application on optoelectronics, sensing, catalysis and photothermal cancer therapy [27–29]. Recent trend in the visible light photocatalytic activity of the SPR nanomaterial enable the charge separation for the effective formation of free radicals, which enhance the photocatalytic activity of the nanomaterial [30–32]. Wang et al. [33] fabricated Au nanoflower printed glassy carbon electron as an electrochemical sensor for the enhanced detection of glycosylated haemoglobin. Similarly, Jandas et al. [34] fabricated Au-MoS₂-rGO nanocluster modified with polyimide as an effective probe for the detection of carcinoembryonic antigen. The wide application enables the recent research to focus on the Au modified nano-heterojunction for the effective detection of various analyte and enhanced photocatalytic activity [32–34]. The present study reports the synthesis and application of Au@Mg bimetallic nanosphere as an effective probe for the photocatalytic degradation of polystyrene and for effective detection of CEF. Here, the proposed method is a non-enzymatic method for the effective detection of CEF.

2. Experimental

2.1. Materials

Instrumental details on the characterization of the synthesised Au@Mg bimetallic nanomaterial are provided in the supplementary material Text S1.

2.2. Synthesis of bimetallic Au@Mg nanospheres

Iliut et al. [35] described an ascorbic acid assisted Au nanoparticle (Au NPs) synthesis. Briefly, 1 mL of HAuCl₄ (10 mM), and 0.5 mL of MgSO₄ (10 mM) were dissolved in 10 mL of distilled H₂O and the solution was stirred for 15 min. Thereafter, 40 µL of ascorbic acid (20 mM) was added to the above solution and the mixture was kept for 30 mins to change to purple colour, which indicate the formation of bimetallic Au@Mg nanospheres.

2.3. Photocatalytic degradation of PS

The photocatalytic degradation of PS (20 mg/L) was performed by irradiation of Au@Mg nanosphere (50 mg/L) under 1000 W halogen lamp in presence of Cl⁻ ion (1 mM). Here, PS solution was prepared by addition of 20 mg of PS in 20 mL ethanol and stirred for 30 min at room temperature, then diluted in distilled H₂O for the effective formation of reactive oxygen species. The photocatalytic degradation of PS was determined by performing total organic compound (TOC) analysis. Every 20 min, 10 mL of the reaction mixture was collected and TOC was per-

formed to determine by presence of PS. Similarly, the photocatalytic degradation was performed in presence of various metal ions (Cl⁻, SO₄²⁻, NO₃⁻, PO₄³⁻ and CO₃²⁻, 1 mM) and the degradation of PS was determined. In addition, the photocatalytic degradation of PS was also performed in absence of metal ions, by varying the nanomaterial concentration (10 to 100 mg/L), by varying the PS concentration (5 to 25 mg/L), and by varying pH 4 to 9 (20 mg/L -PS and 50 mg/L - Au@Mg). To determine the reusability of the Au@Mg nanosphere, the six-cycle photodegradation test was performed. Radical scavenging experiment was performed in presence of isopropyl alcohol (IPA, 1 mL), benzoquinone (BQ - 1 mM, 1 mL), nitrobenzene (NB, 1 mL), ethylenediaminetetraacetic Acid (EDTA - 1 mM, 1 mL) and AgNO₃ for quenching of •OH, O₂•, •OCl, h⁺ and e⁻ respectively [26–28]. The photocorrosion of Au@Mg nanosphere was determined by XRD and XPS analysis after irradiation.

2.4. Spectrophotometric sensing of CEF

The spectrophotometric sensing of CEF by Au@Mg nanosphere was performed by the addition of equal volume (1 mL) of fabricated Au@Mg nanosphere and CEF (1 mM), then the solution was stirred for 10 min and UV-visible absorption spectra was recorded in the range of 300 to 700 nm. The selectivity of the Au@Mg nanosphere was determined by addition of various drugs such as paracetamol, penicillin, tetracycline and cefixime (1 mM). Further, the quantitative analysis was performed by the addition of different concentration of CEF (0.01 nM to 1 mM) and the UV-visible absorption spectra was recorded in the range of 300 to 700 nm. In addition, the mixture of drugs in presence and absence of CEF was added to Au@Mg nanosphere to study the interference of other drug on the detection of CEF. Similarly, the sensing of Au@Mg nanosphere was studied at different volume of CEF (0.1 to 1 mL). The colorimetric detection of CEF by Au@Mg nanosphere was studied under various environmental parameters including pH (5 to 9), temperature (10 to 60 °C) and saline concentration (0.1 to 0.8 %) to determine the stability of environmental sample.

Real sample analysis was performed by spiking the known concentration of CEF on pond water, drinking water, milk, tap water and blood serum. Pond water.

3. Results and discussion

3.1. Characterization of bimetallic Au@Mg nanospheres

Fig. 1a shows the XRD spectrum of Au@Mg nanosphere, which shows the particles are crystalline in nature. The XRD pattern of Au@Mg nanosphere showed peaks at 11.6°, 27°, 38.1°, 44.4°, 64.7° and 77.8°. The peaks at 38.1°, 44.4°, 64.7° and 77.8° correspond to Au NPs [36], whereas the peak at 11.6°, 27°, 44.4° and 77.8° corresponds to Mg [37]. Thus, the XRD results show similar peak at 44.4° and 77.8° for both Mg and Au, which shows the effective formation of Au shell and

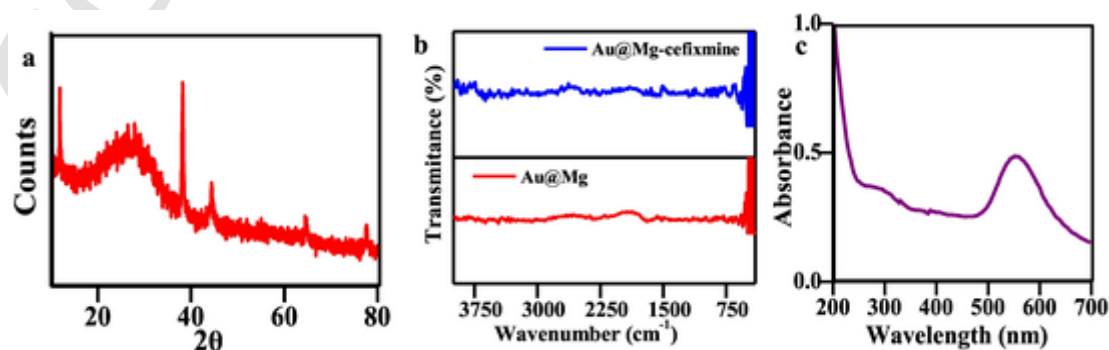


Fig. 1. (a) XRD, (b) FTIR and (c) UV-visible absorption spectra of Au@Mg.

Mg core [29]. The average crystalline size of Au@Mg nanosphere was calculated by Williamson-Hall (W—H) equation and the average particle size was calculated to be 82 nm [38,39]. The Williamson-Hall analysis (WH plot) of Au@Mg nanospheres is displayed in Supplementary material Fig. S1. WH plot is to determine the triple junction developed in the nanocrystals due to the point defect, intrinsic strain and stacking faults. Here, the plot shows that there is no extension or deformation occurred between Au and Mg, which further confirms the formation of nanospheres.

Fig. 1b shows the FTIR spectrum of Au@Mg nanosphere before and after interaction with CEF. The FTIR spectrum of Au@Mg nanosphere shows vibration stretching from 500 to 400 cm^{-1} which corresponds to the metal (Au and Mg) peaks [37]. Here, FTIR spectrum showed peak at 3620 and 1552 cm^{-1} which was due to the OH group stretching [40]. The vibration stretching at 2452 and 1187 cm^{-1} corresponds to the C—H and C=C stretching [40]. The presence of vibration stretching of both metal and organic group shows the effective interaction of CEF with Au@Mg nanospheres. The UV-visible absorption spectra of Au@Mg nanospheres was recorded in the range of 300 to 700 nm and showed λ_{max} at 557 nm, which was due to the electronic excitation of π electron to π^* (Fig. 1c).

Fig. 2a & b shows the TEM image of Au@Mg which shows that prepared particle was spherical in shape. The back shade indicates the Mg core and grey colour indicates the Au shell, which shows the effective formation of Au@Mg nanospheres. The selected area electron diffraction (SAED) pattern of Au@Mg nanosphere shows that the particles are crystalline and polydisperse in nature and it is in accordance with XRD pattern of Au@Mg nanospheres (Fig. 2c). The d-spacing values in SAED with corresponding hkl plane further confirm the formation of Au@Mg nanospheres. SEM image of Au@Mg nanosphere after

the interaction of CEF was depleted in Fig. 2d, which confirms the aggregation of the nanomaterial.

The band gap energy of the nanomaterial was determined by UV-visible DRS spectrum of the nanomaterial. The band gap of the nanomaterial was determined by Kubelka Munk plot by the Eq. (2) [41, 42].

$$F(R) hv^2 = A (hv = E_g) \quad (2)$$

where, E_g represents optical bandgap, v represents frequency of light, h represents Planck constant, A represent frequency of light and F represent Kubelka Munk function. The band gap of Au@Mg nanospheres was found to be 2.59 eV.

Fig. 3a illustrates the XPS spectra of Au@Mg nanospheres, which demonstrates spectrum of Au and Mg. This seems to be well correlated to the TEM and XRD. The XPS spectrum of Au showed sharp peak at 88.3 and 82.4 eV which corresponds to spin $4f_{7/2}$ and $4f_{5/2}$ respectively [33]. The XPS spectrum of Mg showed sharp peak at 1304.1 eV of corresponding spin 1S of band gap energy of 3.2 eV [43]. The result shows the effective formation of Au@Mg nanosphere.

Fig. 3b1 shows the Raman spectrum of Au@Mg nanospheres. The spectrum showed peaks at 260 cm^{-1} indicated the vibration spectrum of Au and the broad spectrum at 1036 cm^{-1} indicate the vibration spectrum of Mg [44,45]. Thus, lower in the peak intensity of Mg than Au shows the effective formation of Au@Mg core shell nanosphere. The Raman spectrum of Au@Mg-CEF showed peaks at 1036, 1352, 1529 and 2135 cm^{-1} which represents the stretching of metal (Mg) and organic group (C—H, C=C and N—O) (Fig. 3b2) [45]. The I_D/I_G before and after interaction with CEF were found to be 0.24 and 0.86 respectively. Thus, the results conclude the effective interaction of CEF with Mg.

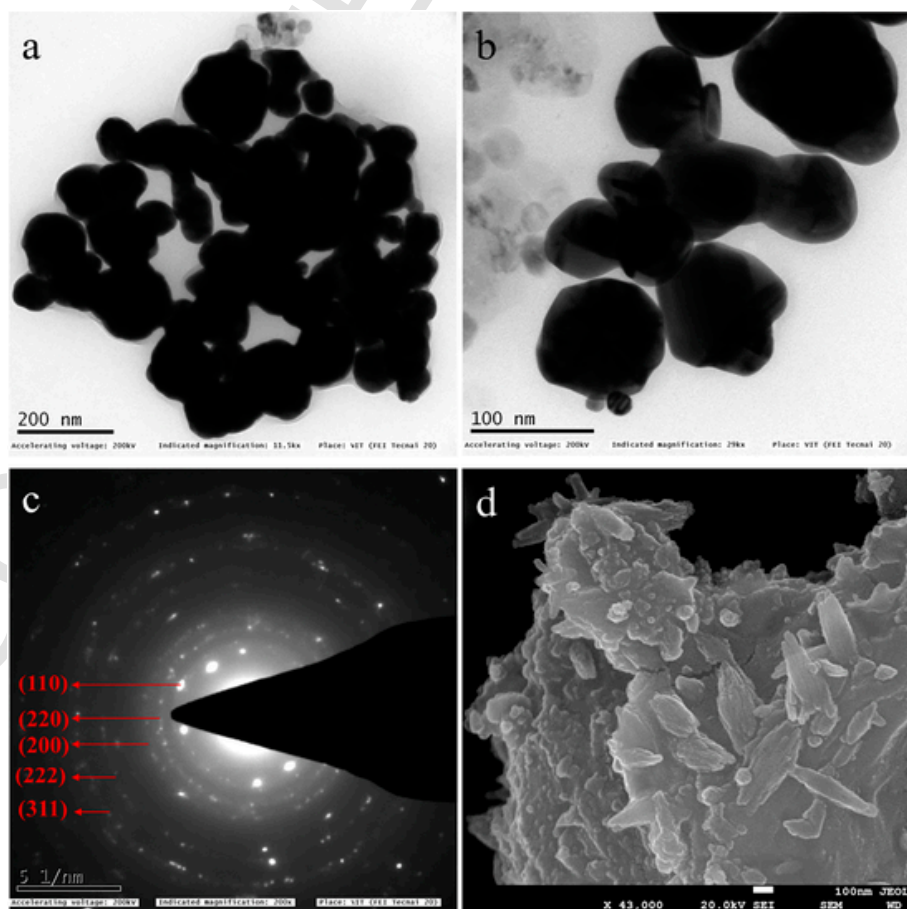


Fig. 2. (a–c) TEM image of Au@Mg, (d) SEM image of Au@Mg after the interaction of cefixime.

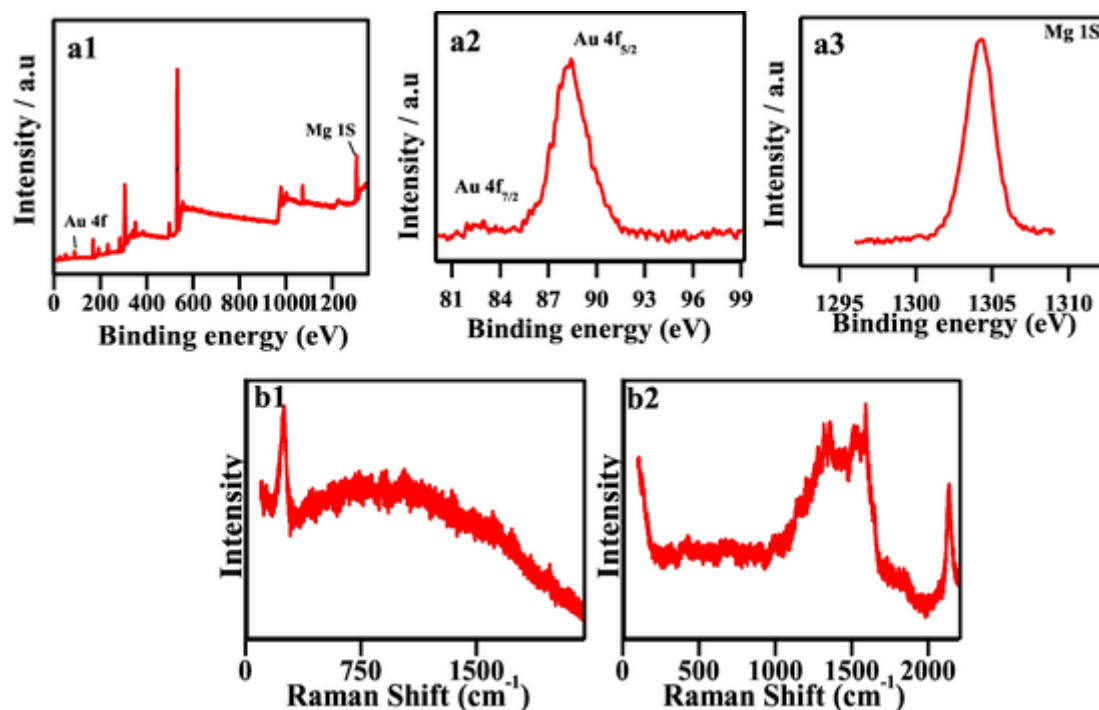


Fig. 3. (a1–a3) XPS spectra of Au@Mg, (b1) Raman spectroscopy of Au@Mg and (b2) Raman spectroscopy of Au@Mg-Cefixime.

3.2. Photocatalytic degradation of PS

The photocatalytic degradation of PS by Au@Mg nanosphere was performed in presence of various ion and the results shows that the PS degradation was effective in presence of Cl^- ion (97.2 %) than SO_4^- , NO_3^- , PO_4^- and CO_3^- ion (Fig. 4a). Here, the degradation efficiency of PS in presence of NO_3^- , PO_4^- and CO_3^- ion showed better performance than in the absence of ions, which seems to contribute to formation of $\bullet\text{OH}$ by undergoing protonation [46,47]. Hence, the higher degradation efficiency of PS was due to the formation of $\text{OCl}\bullet$. The degradation of PS was determined by TOC analysis. TOC analysis showed the gradual reduction of carbon present in the reaction mixture. Nevertheless, the photocatalytic degradation of PS was comparatively lower in absence of ions (Fig. 4c). The rate kinetic of the reaction mixture was determined by the following reaction Equ. 3

$$\ln\left(\frac{C_t}{C_0}\right) = Kt \ln\left(\frac{C_t}{C_0}\right) = Kt \quad (3)$$

where, C_0 and C_t represent the initial concentration and final concentration at time 't'. The rate constant and the regression coefficient of Au@Mg on photocatalytic degradation of PS in presence of Cl^- ions was 0.008 and 0.993 respectively (Fig. 4b). Here, rate constant of photodegradation of PS by Au@Mg nanosphere in presence of ion mixture follows pseudo first order reaction [48,49]. According to the previous

literature, the photocatalytic degradation of PS was found to less than 85 % (Supplementary Material Table S1). Here, the prepared nanomaterial was found to be effective for the complete mineralization of PS.

The photocatalytic degradation of PS was performed under various pH conditions from 5 to 9, was adjusted by using 0.1 NaOH and 0.1 HCl and the degradation was effective at pH 2 (Supplementary material Fig. S2a1 & a2). The lower in the pH enable the effective protonation of the nanomaterial on the effective interaction with PS and thus enables the effective oxidation of organic complex for the complete mineralization of PS. In addition, the acidic pH boost the charge separation due to higher protonation, which interact with Cl^- ions resulting in the formation of $\text{OCl}\bullet$. This radical thereby contributes for the degradation of plastic. Similarly, the photocatalytic reaction was carried out by varying the nanomaterial concentration (10 to 100 mg/L). The results indicate that increasing the nanomaterial concentration enhances the photocatalytic efficiency (Supplementary material Fig. S2b1 & b2). The photocatalytic experiment was repeated in presence of varying PS concentration and the results showed that the lower PS concentration exhibited better performance (Supplementary material Fig. S2c1 & c2). The reusability of the Au@Mg nanosphere was determined by six cycle test and the degradation efficiency was found to be 99.5 %. The difference in the degradation of PS on first and sixth cycle was 0.41 % (Supplementary material Fig. S3a). The radical scavenging experiment was performed in presence of IPA, NB, BQ, AgNO_3 and EDTA and the results

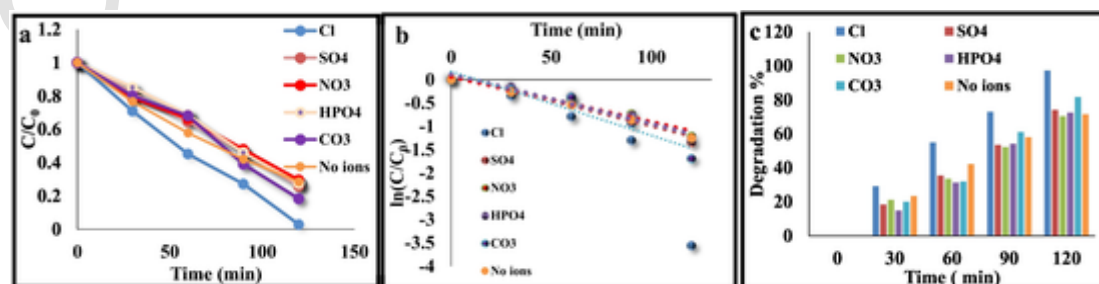


Fig. 4. (a) Plot C/C_0 , (b) $\ln(C/C_0)$ and (c) degradation percentage on photocatalytic degradation of polystyrene by Ag@Mg nanosphere (PS – 20 mg/L, Ions – 1 mM).

shows that OCl^\bullet and $^\bullet\text{OH}$ plays a major role in the effective degradation of PS (Supplementary material Fig. S3b).

3.3. Sensing of CEF

The sensing of CEF by Au@Mg nanosphere was performed by the addition of 1 mL Au@Mg and CEF, and the results shows that the complete loss in the intensity at 557 nm indicates the effective detection of CEF. Fig. 5a shows the selectivity of probe with various drug (paracetamol, penicillin, tetracycline and cefixime), where the disappearance of peak intensity at 557 nm was observed only in presence of CEF and the other drugs exhibited peak at 557 nm. The results show the efficiency of the probe for the selective detection of CEF by Au@Mg nanospheres. Further, the sensitivity study shows the loss in the peak intensity at 557 nm was observed with higher concentration of CEF (Fig. 5b). The complete disappearance of peak at 557 nm was observed at 10 μM and 1 mM. Here, a plot on concentration of CEF vs absorbance of Au@Mg nanosphere at 557 nm was performed to study the linearity and reliability. Fig. 5c shows that the regression co-efficient on the sensitivity analysis was found to be 0.98 which further confirm the good sensing ability of probe on the detection of CEF. In addition, the interference analysis shows the disappearance of peak at 557 nm and it observed only in the drug mixture with CEF and with only in presence of CEF, whereas the disappearance of peak was not observed with drug mixture without CEF (Fig. 5d). It shows that Au@Mg nanosphere towards the detection of CEF was not interfered by other drugs. The detection of CEF was studied by varying the volume of CEF and it was found that the detection was effective at 1 mL of CEF (Supplementary material Fig.

S4). The limit of detection of CEF by Au@Mg nanosphere was calculated by Eq. (4)

$$LOD = \frac{3\sigma}{\text{Slope}} \quad (4)$$

where σ represents the standard deviation and slope represent the absorbance of Au@Mg nanospheres with CEF. The limit of detection of CEF by Au@Mg nanosphere was calculated to be 450 pM (pico-Molar). The detection of CEF by Au@Mg nanospheres was performed under various pH (4 to 9), temperature (20 to 60 °C) and saline concentration (0.1 to 0.8 %). The results show that the detection was effective at pH 6, 10 °C and 0.1 % saline concentration (Supplementary Material Fig. S5).

Real sample analysis by the probe was performed by spiking of CEF with tap water, drinking water, pond water and blood serum. The relative standard deviation on the recovery of spiked CEF on tap water, drinking water and pond was found to be less than 1 %. Further, the detection was tested with blood serum and the recovery % was found to be 99.7 % (Supplementary material Table S2). The results show that the detection probe was found to be an effective tool for the detection of CEF on real sample analysis.

3.4. Photocatalytic mechanism of Au@Mg nanospheres

The graphical representation of the photocatalytic mechanism of Au@Mg nanosphere for the degradation of PS is illustrated in Supplementary material Fig. S6. The plasmonic excitation of electron occurs on Au causing the formation of hot electron and hole pair upon the visible light irradiation [45]. Parallely, the electron form Mg gets excited

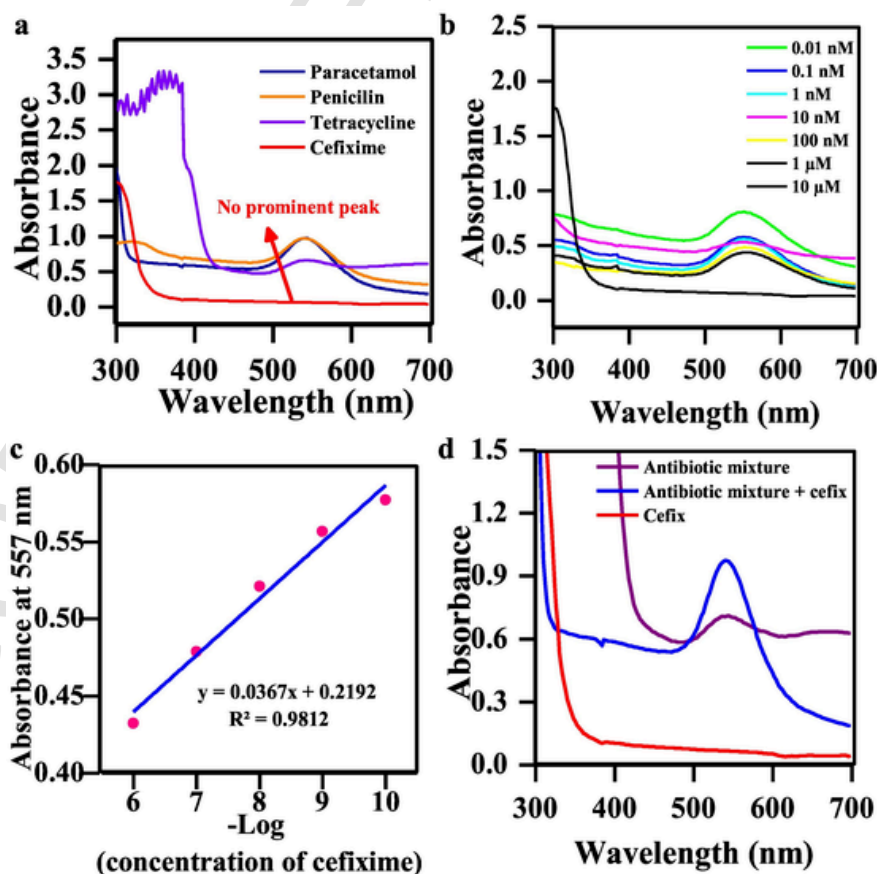


Fig. 5. (a) UV visible spectra on the selective detection of cefixime (1 mL – Au@Mg, various drug 1 mM), (b) UV visible spectra of the sensitive detection of cefixime (0.001 nM to 1 mM) (c) linear plot on absorbance of Au@Mg versus concentration of cefixime (1 mL – Au@Mg, various drug 0.001 nM to 1 mM) and (d) UV visible spectra of interference on detection of cefixime (1 mL – Au@Mg and drug mixture – 1 mM).

and transferred to Au and thus causes the electron hole on Au. The reduction in the oxidation power of Au was mainly due to hot electron and hole pair relax ultrafast for recombination (100 fs to 1 ps) in absence of H₂ or H₂O due to its electron-electron scattering [50]. However, when Au was introduced in H₂O, it enables the migration of hot holes to the hybrid thereby leading to the formation of Au—H resulting in lower recombination rate. The reason for the effective trapping of hot hole and electron pair on inhibiting the oxidation power as follow.

1. The freely localized hot hole is highly delocalized in the mean path range of 20–150 nm [51]. The migration of the hot holes generated by Au to form Au—H hybrid is to form low coordinated positions by the formation of interface or defect. This interface thereby restricts the recombination and results in better photocatalytic performance.

2. According the previous literature, the relaxation of hot holes near to fermi level energy (E_f) is extremely fast [52]. As the hot holes are not thermodynamically favourable, they can uphill the photocatalytic degradation of PS as the d-s antibonding orbital (Au—H hybridization) was lower than the E_f of Au (0.6 eV) [53].

The effective trapping of the hot hole on the migration of Au—H enables the effective photocatalytic degradation of PS [54,55]. The entrapment of hot holes from Au to Au—H enables the formation of radical which enhance the photocatalytic activity of the metallic nanoparticle.

3.5. Photocatalytic degradation pathway of polystyrene

The photocatalytic degradation pathway of PS by Au@Mg nanosphere is illustrated in Supplementary material Fig. S7. The reactive site interaction of the free radical, nucleophilic attack and electrophilic attack on cefixime was determined by Fukui function performed by DMol3. The electron charge density and E_{abs} of Au@Mg nanosphere was higher than with water (E_{abs} of NPs with PS > E_{abs} of NPs), which shows the effective formation of charge density. Here, the radical attack and chloride radical occurs on the C2 and C4 of PS. The radical attack on the degradation of PS causes the formation of intermediate (methyl acetophenone, hydroquinone, formic acid, acetophenone, phenol, phenylpropionic acid and methylbenzaldehyde) and further oxidizes to form CO₂ and H₂O. Further, the radical and nucleophilic attack cleaves the benzene ring resulting in the formation of the intermediates and the extensive interaction of the radical on PS causes the formation of intermediates. The complete mineralization of the PS resulted in the formation of CO₂ and H₂O.

3.6. Mechanism of the detection of CEF by Au@Mg nanosphere

The graphical representation of Au@Mg nanosphere towards the detection of CEF is illustrated in Supplementary material Fig. S9. Here, Mg core interact with CEF to form a metal CEF complex and thus causes the aggregation of the nanomaterial [56,57]. The zeta potential of Au@Mg and Au@Mg-CEF was found to -32.9 ± 18.8 and -19.4 ± 15.3 mV, and the aggregation was due to the formation of metal drug complex which causes the loss in the absorbance of nanomaterial at 557 nm.

The XPS spectrum of Au@Mg-CEF was performed to determine the effective interaction site and it is shown in Supplementary material Fig. S8. The XPS spectra of Au 4f showed sharp peak at 88.3 and 82.4 eV [33]. The XPS spectrum of Mg 1S showed peak at 1304.3 eV [43]. Here, the peak at 283.1, 530.7 and 389.1 eV represent presence of C, O and N with orbital spin of 1S confirms the effective interaction of Au@Mg nanosphere with CEF. Here the presence of C, N and O after the interaction of CEF, shows the effective interaction of CEF with Au@Mg nanospheres and thus causes the aggregation of Au@Mg nanospheres.

The DFT analysis of Au@Mg nanosphere was performed to determine the electronic band structure, DOS and work function (Supplementary material Fig. S9). The electronic band structure, DOS and work

function shows the effective electron transfer between Au and Mg. The work function of cefixime was calculated to be 4.28 eV, the work function of Au and Mg was calculated to be 3.65 eV and 5.46 eV respectively [57–60]. The higher in the work function of Mg than Au causes the effective interaction with CEF to form metal drug complex.

4. Genotoxic

The genotoxicity of PS before and after photocatalytic degradation was performed by using root tip of *A. cepa*. Briefly, 20 mg of PS was dissolved in ethanol and the cytotoxicity was determined. Similarly, PS reaction mixture was prepared and 100 mg/L of Au@Mg nanospheres were augmented and irradiated under visible light. Then, the irradiated reaction mixture was centrifuged, the nanospheres were collected and the cytotoxicity of the degraded product was performed against *A. cepa*. The results show that the cytotoxicity of PS before degradation was significantly higher than after degradation (Supplementary material Tables S3 and S4). The formation of the disturbed interference on mitosis cycle causes the inhibition of DNA and protein synthesis and thus cytotoxicity of the nanocomposite was determined [48]. The micronuclei index of PS after degradation was comparatively lower than that of before degradation. The higher in the micronuclei index indicate the higher in the genotoxicity against *A. cepa*. The lower in the toxicity of PS contaminated water after degradation was due to the complete mineralization of the PS on the formation of non-toxic product. The results suggest that Au@Mg nanosphere was effective on the photocatalytic degradation of PS and it does not show considerable genotoxicity on environmental organism. Hence, Au@Mg nanospheres can be used as an effective tool for the treatment of plastic contaminated water and the treated water was found to be an eco-friendly to the environment.

5. Conclusions

In summary, Au@Mg nanosphere was fabricated by chemical reduction method and it served as a rapid and good sensor for CEF detection. Here, the prepared nanospheres were crystalline and polydisperse with average particle size of 82 nm. The photocatalytic degradation of polystyrene by Au@Mg was studied and the effective degradation was found to be 97.1 % (in presence of chlorine ions). The PS degradation was studied in presence and absence of different metal ions, where the detection was effective in presence of chlorine ions. Further, reusability study was performed and the results shows that Au@Mg nanospheres can be used for long term. The genotoxicity of the polystyrene was studied before and after degradation which haven't exhibited considerable toxic effects. The prepared probe showed selective and sensitive detection towards CEF. The presence of other drug did not interfere in the detection of CEF by Au@Mg nanosphere. The limit of detection of CEF by Au@Mg nanospheres was calculated to be 450 pM. The real sample analysis was performed with the blood serum and the recovery % was found to be 99.7 %. Thus, the results conclude that the bimetallic Au@Mg nanosphere serves as an effective tool for the monitoring and optimization of CEF drug and for photocatalytic degradation of polystyrene.

Declaration of competing interest

No conflict.

Data availability

Data will be made available on request.

Acknowledgment

The authors extend their appreciation to the Researchers Supporting Project number (RSP-2022/483) King Saud University, Riyadh, Saudi Arabia.

Appendix A. Supplementary data

Supplementary data to this article can be found online at <https://doi.org/10.1016/j.jwpe.2022.103350>.

References

- [1] F. Akhgari, N. Samadi, K. Farhadi, Fluorescent carbon dot as nanosensor for sensitive and selective detection of cefixime based on inner filter effect, *J. Fluoresc.* 27 (2017) 921–927.
- [2] R. Biczak, B. Pawłowska, P. Balczewski, P. Rychter, The role of the anion in the toxicity of imidazolium ionic liquids, *J. Hazard. Mater.* 274 (2014) 181–190.
- [3] J. Shah, M.R. Jan, M. Yousaf, Cadmium sulfide quantum dots as a fluorescent probe for quantitative determination of cefixime, *J. Appl. Spectrosc.* 83 (2016) 248–253.
- [4] A. Dubala, J.S.K. Nagarajan, C.S. Vimal, R. George, Simultaneous liquid chromatography–mass spectrometry quantification of cefixime and clavulanic acid in human plasma, *J. Chromatogr. Sci.* 53 (2015) 694–701.
- [5] F. Meng, X. Chen, Y. Zeng, D. Zhong, Sensitive liquid chromatography–tandem mass spectrometry method for the determination of cefixime in human plasma: application to a pharmacokinetic study, *J. Chromatogr. B* 819 (2005) 277–282.
- [6] B. Singh, D. Parwate, S. Srivastava, S. Shukla, Thin-layer chromatographic selective and stability-indicating method for assay of cefixime in pharmaceuticals, *PC J. Planar Chromatogr. - Mod. TLC* 24 (2011) 524–528.
- [7] S. Ghattavi, A. Nezamzadeh-Ejhieh, A brief study on the boosted photocatalytic activity of AgI/WO₃/ZnO in the degradation of methylene blue under visible light irradiation, *Desalin. Water Treat.* 166 (2019) 92–104.
- [8] N. Omrani, A. Nezamzadeh-Ejhieh, A ternary Cu₂O/BiVO₄/WO₃ nano-composite: scavenging agents and the mechanism pathways in the photodegradation of sulfasalazine, *J. Mol. Liq.* 315 (2020) 113701.
- [9] A.O. Alnajjar, Simultaneous determination of ofloxacin and cefixime in tablet formulation using capillary electrophoresis, *J. Liq. Chromatogr. Relat. Technol.* 36 (2013) 2687–2697.
- [10] N. Bukhari, A.A. Al-Warthan, S.M. Wabaidur, Z.A. Othman, M. Javid, S. Haider, Spectrofluorimetric determination of cefixime in pharmaceutical preparation and biological fluids using calcein as a fluorescence probe, *Sens. Lett.* 8 (2010) 280–284.
- [11] A.A. Elbashir, S.M.A. Ahmed, H.Y. Aboul-Enein, New spectrofluorimetric method for determination of cephalosporins in pharmaceutical formulations, *J. Fluoresc.* 22 (2012) 857–864.
- [12] S.O. Tümay, V. Şanko, E. Demirbas, A. Şenocak, Fluorescence determination of trace level of cadmium with pyrene modified nanocrystalline cellulose in food and soil samples, *Food Chem. Toxicol.* 146 (2020) 111847.
- [13] N. Karimian, M. Gholivand, G. Malekzadeh, Cefixime detection by a novel electrochemical sensor based on glassy carbon electrode modified with surface imprinted polymer/multiwall carbon nanotubes, *J. Electroanal. Chem.* 771 (2016) 64–72.
- [14] A.A. Ensafi, A.R. Allafchian, Multiwall carbon nanotubes decorated with NiFe₂O₄ magnetic nanoparticles, a new catalyst for voltammetric determination of cefixime, *Colloids Surf. B Biointerfaces* 102 (2013) 687–693.
- [15] F. Akhgari, N. Samadi, K. Farhadi, Fluorescent carbon dot as nanosensor for sensitive and selective detection of cefixime based on inner filter effect, *J. Fluoresc.* 27 (2017) 921–927.
- [16] H. Eskandari, M. Amirzehni, H. Asadollahzadeh, P.A. Eslami, Molecularly imprinted polymers on CdS quantum dots for sensitive determination of cefixime after its preconcentration by magnetic graphene oxide, *New J. Chem.* 41 (2017) 7186–7194.
- [17] H. Al-Zawaidah, D. Ravazzolo, H. Friedrich, Macroplastics in rivers: present knowledge, issues and challenges, *Environ Sci Process Impacts* 23 (2021) 535–552.
- [18] N. Omrani, A. Nezamzadeh-Ejhieh, A comprehensive study on the mechanism pathways and scavenging agents in the photocatalytic activity of BiVO₄/WO₃ nano-composite, *J. Water Process Eng.* 33 (2020) 101094.
- [19] N. Arabpour, A.L. Nezamzadeh-Ejhieh, Modification of clinoptilolite nanoparticles with iron oxide: increased composite catalytic activity for photodegradation of cotrimaxazole in aqueous suspension, *Mater. Sci. Semicond. Process.* 31 (2015) 684–692.
- [20] M. Nosuhi, A. Nezamzadeh-Ejhieh, Comprehensive study on the electrocatalytic effect of copper – doped nano-clinoptilolite towards amoxicillin at the modified carbon paste electrode – solution interface, *J. Colloid Interface Sci.* 497 (2017) 66–72.
- [21] E. Shahnazari-Shahrezaie, A. Nezamzadeh-Ejhieh, A zeolite modified carbon paste electrode based on copper exchanged clinoptilolite nanoparticles for voltammetric determination of metronidazole, *RSC Adv.* 7 (2017) 14247–14253.
- [22] S. Thakkar, J. Liu, L.F. Duméed, B.R. Singh, S. Shukla, W. Yang, Arsenic ion assisted core-satellites nano-assembly of gold nanoparticles for its colorimetric determination in water, *J. Water Process Eng.* 48 (2022) 102833.
- [23] V. Bagalkot, L. Zhang, E. Levy-Nissenbaum, S. Jon, P.W. Kantoff, R. Langer, O.C. Farokhzad, Quantum dot– aptamer conjugates for synchronous cancer imaging, therapy, and sensing of drug delivery based on bi-fluorescence resonance energy transfer, *Nano Lett.* 7 (2007) 3065–3070.
- [24] B.M. May, O.J. Fakayode, K.N. Mashale, M.F. Bambo, A.K. Mishra, E.N. Nxumalo, Detection and separation of silver ions from industrial wastewaters using fluorescent d-glucose carbon nanosheets and quaternary silver indium zinc sulphide quantum dots, *J. Water Process Eng.* 49 (2022) 102944.
- [25] L. Kong, J. Chen, M. Huang, GO/Au@Agnanobones decorated membrane for simultaneous enrichment and on-site SERS detection of colorants in beverages, *Sensors Actuators B Chem.* 344 (2021) 130163.
- [26] S. Ghattavi, A. Nezamzadeh-Ejhieh, A visible light driven AgBr/g-C₃N₄ photocatalyst composite in methyl orange photodegradation: focus on photoluminescence, mole ratio, synthesis method of g-C₃N₄ and scavengers, *Compos. Part B* 183 (2020) 107712.
- [27] S. Ghattavi, A. Nezamzadeh-Ejhieh, A double-Z-scheme ZnO/AgI/WO₃ photocatalyst with high visible light activity: experimental design and mechanism pathway in the degradation of methylene blue, *J. Mol. Liq.* 322 (2021) 114563.
- [28] N. Omrani, A. Nezamzadeh-Ejhieh, Focus on scavengers' effects and GC-MASS analysis of photodegradation intermediates of sulfasalazine by Cu₂O/CdS nanocomposite, *Sep. Purif. Technol.* 235 (2020) 116228.
- [29] P. Bhatia, M. Nath, Nanocomposites of ternary mixed metal oxides (Ag₂O/NiO/ZnO) used for the efficient removal of organic pollutants, *J. Water Process Eng.* 49 (2022) 102961.
- [30] H. Derikvandi, A. Nezamzadeh-Ejhieh, Increased photocatalytic activity of NiO and ZnO in photodegradation of a model drug aqueous solution: effect of coupling, supporting, particles size and calcination temperature, *J. Hazard. Mater.* 321 (2017) 629–638.
- [31] P. Mohammadyari, A. Nezamzadeh-Ejhieh, Supporting of mixed ZnS–NiS semiconductors onto clinoptilolite nano-particles to improve its activity in photodegradation of 2-nitrotoluene, *RSC Adv.* 5 (2015) 75300–75310.
- [32] S.A. Mirsalari, A. Nezamzadeh-Ejhieh, A.R. Massah, A designed experiment for CdS-AgBr photocatalyst toward methylene blue, *Environ. Sci. Pollut. Res.* 29 (2022) 33013–33032.
- [33] N.S. Shah, J. Iqbal, M. Sayed, S. Rau, M.D. Albaqami, J.A. Khan, Z.U.H. Khan, F. Rehman, A. Khan, M. Naseem, A.I. Hashmi, Ionic liquid functionalized nano-zerovalent cerium for catalytic degradation of carbamazepine and colorimetric sensing of H₂O₂, *J. Water Process Eng.* 40 (2021) 101964.
- [34] P.J. Jandas, J. Luo, K. Prabakaran, F. Chen, Y. QingFu, Highly stable, love-mode surface acoustic wave biosensor using Au nanoparticle-MoS₂-rGO nano-cluster doped polyimide nanocomposite for the selective detection of carcinoembryonic antigen, *Mater. Chem. Phys.* 246 (2020) 122800.
- [35] M. Iliut, C. Leordean, V. Canpean, C.M. Teodorescu, S. Astilean, A new green, ascorbic acid-assisted method for versatile synthesis of Au–graphene hybrids as efficient surface-enhanced Raman scattering platforms, *J. Mater. Chem. C* 1 (2013) 4094–4104.
- [36] L. Chen, H.Y. Wang, Y. Li, M. Zha, Q.C. Jiang, Morphology and size control of octahedral and cubic primary Mg₂Si in an Mg–Si system by regulating Sr contents, *CrytEngComm* 16 (2014) 448–454.
- [37] S.A. El-Hakam, A.A. Ibrahim, L.A. Elatwy, W.S. AboEl-Yazeed, R.S. Salama, Y.G. AbouEl-Reash, A.I. Ahmed, Greener route for the removal of toxic heavy metals and synthesis of 14-aryl-14H dibenzo[a, j] xanthene using a novel and efficient ag-mg bimetallic MOF as a recyclable heterogeneous nanocatalyst, *J. Taiwan Inst. Chem. Eng.* 122 (2021) 176–189.
- [38] M. Rezaei, A. Nezamzadeh-Ejhieh, The ZnO–NiO nano-composite: a brief characterization, kinetic and thermodynamic study and study the arrhenius model on the sulfasalazine photodegradation, *Int. J. Hydrog. Energy* 45 (2020) 24749–24764.
- [39] T. Tamiji, A. Nezamzadeh-Ejhieh, Electrocatalytic behavior of AgBr NPs as modifier of carbon past electrode in the presence of methanol and ethanol in aqueous solution: a kinetic study, *J. Taiwan Inst. Chem. Eng.* 104 (2019) 130–138.
- [40] Y. Yao, B. Gao, J. Chen, L. Yang, Engineered biochar reclaiming phosphate from aqueous solutions: mechanisms and potential application as a slow-release fertilizer, *Environ. Sci. Technol.* 47 (2013) 8700–8708.
- [41] H. Derikvandi, A. Nezamzadeh-Ejhieh, A comprehensive study on enhancement and optimization of photocatalytic activity of ZnS and SnS₂: response surface methodology (RSM), n-n heterojunction, supporting and nanoparticles study, *J. Photochem. Photobiol. A Chem.* 348 (2017) 68–78.
- [42] F. Soori, A. Nezamzadeh-Ejhieh, Synergistic effects of copper oxide-zeolite nanoparticles composite on photocatalytic degradation of 2,6-dimethylphenol aqueous solution, *J. Mol. Liq.* 255 (2018) 250–256.
- [43] M.K. Chuang, S.S. Yang, F.C. Chen, Metal nanoparticle-decorated two-dimensional molybdenum sulfide for plasmonic-enhanced polymer photovoltaic devices, *Materials* 8 (2015) 5414–5425.
- [44] Y. Ma, J. Ding, L. Chan, J. Yi, T.S. Herrg, S. Huang, X. Huang, Room temperature ferromagnetism in (Zn_{1-x}, Mg_x)O film, *IEEE Trans. Magn.* 46 (2010) 1338–1341.
- [45] M.L. Brongersma, N.J. Halas, P. Nordlander, Plasmon-induced hot carrier science and technology, *Nat. Nanotechnol.* 10 (2015) 25–34.
- [46] S.A. Mirsalari, A. Nezamzadeh-Ejhieh, Focus on the photocatalytic pathway of the CdS-AgBr nano-catalyst by using the scavenging agents, *Sep. Purif. Technol.* 250 (2020) 117235.
- [47] S. Senobari, A. Nezamzadeh-Ejhieh, A comprehensive study on the photocatalytic activity of coupled copper oxide-cadmium sulfide nanoparticles, *Spectrochim. Acta A Mol. Biomol. Spectrosc.* 196 (2018) 334–343.
- [48] M. Mehrli-Afjani, A. Nezamzadeh-Ejhieh, H. Aghaei, A brief study on the kinetic aspect of the photodegradation and mineralization of BiOI-Ag₃PO₄ towards

- sodium diclofenac, Chem. Phys. Lett. 759 (2020) 137873.
- [49] A. Norouzi, A. Nezamzadeh-Ejhieh, Preparation, characterization, and investigation of the catalytic property of α -Fe₂O₃-ZnO nanoparticles in the photodegradation and mineralization of methylene blue, Chem. Phys. Lett. 752 (2020) 137587.
- [50] M.P. Seah, W.A. Dench, Quantitative electron spectroscopy of surfaces: a standard data base for electron inelastic mean free paths in solids, Surf. Interface Anal. 1 (1979) 2–11.
- [51] K.W. Frese, C. Chen, Theoretical models of hot carrier effects at metal-semiconductor electrodes, J. Electrochem. Soc. 139 (1992) 3234–3243.
- [52] A.M. Brown, R. Sundararaman, P. Narang, W.A. Goddard, H.A. Atwater, Nonradiative plasmon decay and hot carrier dynamics: effects of phonons, surfaces, and geometry, ACS Nano 10 (2016) 957–966.
- [53] R. Sundararaman, P. Narang, A.S. Jermyn, W. A, L.I.I. Goddard, H.A. Atwater, heoretical predictions for hot-carrier generation from surface plasmon decay, Nat. Commun. 5 (2014) 5.
- [54] B. Hammer, J.K. Norskov, Why gold is the noblest of all the metals, Nature 376 (6537) (1995) 238–240.
- [55] H. Lee, K. Song, M. Lee, J.Y. Park, In situ visualization of localized surface plasmon resonance-driven hot hole flux, Adv. Sci. 7 (2020) 2001148.
- [56] S. Rubel, S. Akij, Islam, complexation and interaction study of antibiotic cefixime with essential metals by spectrophotometric method, Edelweiss Pharm. Anal. Acta (2020), <https://doi.org/10.33805/2689-9477.104>.
- [57] Y. Mehmood, S. Ghafoor, H. Riaz, R.K. Mahmood, A. Kashif, A. Malik, A. Tariq, H. Yousaf, S.A. Raza, Synthesis, analysis and biological studies of transition metal complexes of cefixime, Int. J. Biosci. 14 (2019) 63–76.
- [58] N.Y.S. Diki, G.K. Gbassi, A. Ouedraogo, M. Berte, A. Trokourey, Aluminum corrosion inhibition by cefixime drug: experimental and DFT studies, J. Electrochem. Sci. Eng. 8 (2018).
- [59] P.T. Sprunger, E.W. Plummer, An experimental study of the interaction of hydrogen with the Mg(0001) surface, Chem. Phys. Lett. 187 (1991) 559–564.
- [60] N. Miura, T. Nanjo, M. Suita, T. Oishi, Y. Abe, T. Ozeki, H. Ishikawa, T. Egawa, T. Jimbo, Solid State Electron. 48 (2004) 689–695.